processes

MDPI

Article

A Data-Driven Framework for Fault Diagnostics in Gearbox Health Monitoring Under Non-Stationary Conditions

Nhan-Phuc Hoang [1], Trong-Du Nguyen [1,*], Tuan-Hung Nguyen [2], Duong-Hung Pham [3], Phong-Dien Nguyen [1] and Thi-Van-Huong Nguyen [1]

[1] ITD Lab, School of Mechanical Engineering, Hanoi University of Science and Technology, Hanoi 100000, Vietnam
[2] School of Engineering and Built Environment, Griffith University, Gold Coast, QLD 4215, Australia
[3] IRIT Laboratory, Toulouse University, and CNRS (UMR5505), 31400 Toulouse, France
* Correspondence: du.nguyentrong@hust.edu.vn

Abstract: Monitoring gearbox health is essential in industrial systems, where undetected faults can result in costly downtime and severe equipment damage. While vibration-based diagnostics are widely utilized for fault detection, analyzing large-scale, non-stationary vibration signals remains a computational challenge, particularly in real-time and resource-constrained environments. This paper presents Data-Driven Synchrosqueezing-based Signal Transformation (DSST), a novel time-frequency method that integrates synchrosqueezing transform (SST) with structured downsampling in both time and frequency domains. DSST significantly reduces computational and memory demands, while preserving high-resolution representations of fault-related features such as gear meshing frequency sidebands and their harmonics. In contrast to prior SST variants, DSST emphasizes diagnostic interpretability, invertibility, and compatibility with data-driven learning models, making it suitable for deployment in modern condition monitoring frameworks. Experimental results on non-stationary gearbox vibration data demonstrate that DSST achieves comparable diagnostic accuracy to conventional SST methods, with substantial gains in processing efficiency—thereby supporting scalable, real-time industrial health monitoring. Unlike existing downsampling-based SST methods, DSST is designed as a diagnostic component within a scalable, data-driven framework, supporting real-time analysis, signal reconstruction, and downstream machine learning integration.

Keywords: gear fault diagnosis; synchrosqueezing transform; time–frequency analysis; downsampling; non-stationary signal; large-scale vibration data; real-time condition monitoring

check for updates

Academic Editor: Xiong Luo

Received: 13 April 2025
Revised: 16 May 2025
Accepted: 21 May 2025
Published: 26 May 2025

Citation: Hoang, N.-P.; Nguyen, T.-D.; Nguyen, T.-H.; Pham, D.-H.; Nguyen, P.-D.; Nguyen, T.-V.-H. A Data-Driven Framework for Fault Diagnostics in Gearbox Health Monitoring Under Non-Stationary Conditions. *Processes* **2025**, *13*, 1663. https://doi.org/10.3390/pr13061663

Copyright: © 2025 by the authors. Licensee MDPI, Basel, Switzerland. This article is an open access article distributed under the terms and conditions of the Creative Commons Attribution (CC BY) license (https://creativecommons.org/licenses/by/4.0/).

1. Introduction

Diagnosing gear faults is crucial for maintaining machinery and ensuring its reliability [1]. Gears are vital in mechanical systems, transmitting power and motion, which makes accurate fault diagnosis essential [2,3]. Their significant role in mechanical failures under various operating conditions further emphasizes this need [4]. Undetected gear faults may trigger further failures throughout the transmission system. However, most current diagnostic approaches are designed for stationary operation conditions, and there is a notable lack of practical tools for identifying gear faults under non-stationary conditions with fluctuating loads and speeds [5]. Gearboxes are among the most essential mechanical components in rotating machinery, playing a vital role in power transmission and overall system efficiency [6,7]. However, these components are frequently subjected to varying

load conditions, changing rotational speeds, and harsh environmental factors, making them particularly vulnerable to faults and degradation [8,9]. Gearbox failures often result in extensive maintenance requirements, unexpected downtime, safety hazards, and even secondary failures in adjacent mechanical components [10,11]. Gearbox failures in real-world applications such as wind turbines, heavy-duty robotics, and automated manufacturing lines can spread through networked systems, resulting in cascading downtime across whole operations. Detecting even a little gear degradation across diverse speed profiles is crucial for condition-based maintenance and operational safety. These operational considerations highlight the significance of developing effective, responsive, and accurate fault diagnostic devices that can operate independently in non-stationary contexts.

Non-stationary vibration signals, often encountered during start-up, shutdown, load variation, or speed ramping, are notoriously difficult to analyze using conventional signal processing techniques [12–14]. Traditional frequency-domain methods, such as the Fourier Transform (FT) [15,16], rely on the assumption of signal stationarity and thus fail to capture the temporal evolution of fault characteristics. While time-domain statistical features and envelope analysis remain widely used, they often lack robustness under variable-speed conditions [17,18]. They may not offer sufficient resolution to detect early-stage or compound faults. Furthermore, non-stationary vibration signals frequently comprise short-lived transient bursts, frequency modulations, and mode interactions that are suppressed under linear or globally stationary [19,20]. Thus, successful diagnostics necessitate time–frequency resolution, tolerance to temporal energy fluctuations, and structure-aware signal encoding.

Time–frequency analysis (TFA) [21,22] has emerged as a robust framework for characterizing non-stationary signals to address these challenges. Classical approaches such as the Short-Time Fourier Transform (STFT) [23] and Continuous Wavelet Transform (CWT) [24,25] provide joint representations of time and frequency, allowing for the identification of transient or modulated signal components. However, both techniques have intrinsic limitations that hinder their applicability in complex scenarios. STFT uses a fixed-size window, which forces a compromise between time and frequency resolution. This limitation makes it unsuitable for signals with multiple frequency components that evolve at different rates. On the other hand, CWT offers a scale-adaptive decomposition, which improves multiresolution analysis but often results in energy smearing, poor localization of rapidly varying components, and difficulty in reconstructing the original signal.

To overcome the resolution trade-offs of classical techniques, reassignment methods such as the reassigned spectrogram and synchrosqueezing transforms (SST) [26–29] were developed. These methods reallocate energy in the time–frequency plane to reflect the instantaneous frequency content more accurately. SST, in particular, preserves the invertibility of the transformation, enabling improved signal reconstruction and more precise separation of overlapping modes. Among these, the Fourier-based Synchrosqueezing Transform (FSST) [27] stands out due to its ability to sharpen spectral representations without departing from the Fourier framework, making it suitable for mechanical fault detection. Furthermore, high-order variants such as High-Order Synchrosqueezing Tranforms [30,31] offer additional benefits in capturing closely spaced components and improving resistance to noise. Despite their strong analytical performance, high-resolution TFA methods like FSST are computationally demanding. Their reliance on dense time-frequency grids and exhaustive reassignment operations poses a significant challenge for processing long-duration signals or implementing real-time diagnostics in embedded systems. The trade-off between diagnostic resolution and computational cost becomes increasingly pronounced in practical industrial environments, where hundreds of machines might be monitored simultaneously. Moreover, hardware limitations can further constrain high-resolution TFA methods, especially in edge devices or low-power industrial controllers. While modern computational

architectures can support deep learning-based fault classification, the high dimensionality and memory consumption of traditional time–frequency representations can still hinder deployment at scale. Therefore, there is a clear need for TFA methods that maintain diagnostic fidelity while reducing computational complexity and memory footprint.

A novel data-driven framework for gearbox fault diagnostics under non-stationary conditions is needed to bridge the gap between analytical robustness and operational scalability. Central to this framework is the Data-Driven Synchrosqueezing-based Signal Transformation (DSST)—a lightweight, scalable, and resolution-preserving method that integrates synchrosqueezing theory with structured downsampling strategies. The DSST algorithm is designed to retain the high-resolution characteristics of SST while minimizing computational overhead, enabling its integration into real-time monitoring systems and machine learning-based diagnostic pipelines. The DSST framework addresses key weaknesses in existing TFA methods through two main innovations. First, it retains the precision of SST in concentrating spectral energy along instantaneous frequency ridges, thereby preserving fault-sensitive information even in the presence of transient and overlapping components. Second, it introduces principled downsampling in both time and frequency domains to reduce the size of the time-frequency matrix, focusing computational resources on signal regions that carry the most relevant diagnostic information.

Recent studies have attempted to reduce the computational load of synchrosqueezing by incorporating downsampling strategies. For instance, a downsampling-based SST [32] was proposed to accelerate time–frequency analysis in large-scale vibration datasets, demonstrating significant reductions in processing time while preserving critical diagnostic features. Although it offers significant improvements in computational efficiency, it remains limited in terms of practical applicability to real-world diagnostics. The method primarily prioritizes algorithmic formulation and mathematical efficiency, without addressing interpretability, real-time deployment, or integration into data-driven diagnostic systems. It does not demonstrate signal reconstruction in an industrial context, nor does it extract fault-specific features such as gear meshing frequency (GMF) harmonics or sidebands from actual vibration data. This study overcomes the limitations of that work by proposing a Data-Driven Synchrosqueezing-based Signal Transformation (DSST), which retains the high-resolution properties of SST while introducing structured downsampling and reconstruction strategies tailored for gearbox fault diagnosis under non-stationary conditions. Unlike previous approaches, DSST is formulated as an interpretable and scalable diagnostic module that is compatible with machine learning frameworks and suitable for peripheral deployment in modern condition monitoring systems.

In contrast, the proposed framework in this work extends beyond computational efficiency. It incorporates structured sparsity in both time and frequency dimensions, maintains invertibility for signal reconstruction, and is specifically designed to output compact, interpretable features that can be directly integrated into data-driven diagnostic models. Furthermore, DSST is formulated as part of a broader fault diagnostic pipeline, explicitly targeting rotating machinery operating under non-stationary conditions, emphasizing edge-deployable and learning-friendly representations.

Furthermore, the invertibility of DSST enables it to serve as a foundational component of hybrid frameworks that combine interpretability and automation. By allowing signal reconstruction from its sparse representation, the technique aids applications that require explainability and traceability, such as in safety-critical or regulated situations. It also enables effective storage and transfer of diagnostic data across remote systems. The modular design of DSST allows smooth integration into multimodal condition monitoring architectures. Its tiny outputs can be used as low-latency input for learning-based anomaly detectors or combined with data from other sources, such as acoustic emissions or motor

current signals, to improve diagnostic accuracy. From a broader perspective, the proposed DSST is consistent with the growing demand for edge-compatible fault diagnosis systems in Industry 4.0 environments. The lower computing load of DSST makes it easier to implement on embedded platforms and supports predictive maintenance scenarios that require rapid judgments. The method's compliance with real-time inference makes it more suitable for closed-loop control systems, where fault identification must be quick and less invasive.

To summarize, the DSST algorithm combines theoretical rigor and technical applicability. It retains the analytical advantages of synchrosqueezing, while resolving the limitations that prevent high-resolution TFA approaches from scaling to industrial-scale installations. Compared to existing works that treat downsampled SST as a standalone signal processing method, DSST is framed as a cohesive diagnostic module within a broader data-driven framework. This architectural distinction ensures compatibility with emerging intelligent monitoring systems that demand computational efficiency and traceable and machine-interpretable features. Finally, DSST fills a significant gap in the field: balancing analytical integrity with computing feasibility. As industrial systems grow in complexity and data volume, lightweight yet exact approaches will become increasingly crucial for providing rapid, interpretable, and autonomous problem diagnostics.

The remainder of this paper is organized as follows: Section 2 presents the mathematical foundation of synchrosqueezing and details the formulation of the DSST algorithm, including downsampling principles and reconstruction capabilities. Section 3 presents the experimental setup, and the datasets used for validation, followed by the benchmarking protocols and evaluation metrics. It then discusses the obtained results, emphasizing the diagnostic accuracy of DSST, its computational efficiency, and its applicability to non-stationary operating conditions. Finally, Section 4 concludes the paper with insights on limitations, industrial deployment considerations, and avenues for future research, including adaptive resolution control, hybrid learning-based frameworks, and multi-source signal fusion.

2. Methodology

To effectively analyze non-stationary vibration signals under varying operating conditions, a combination of classical time-frequency methods and a novel downsampling-based synchrosqueezing approach is employed. The methodology focuses on improving time–frequency resolution while maintaining computational efficiency for large-scale diagnostic applications.

2.1. Short-Time Fourier Transform

STFT is a powerful tool for analyzing non-stationary signals, allowing for simultaneous analysis in both time and frequency domains [33]. This is achieved by dividing the signal into short segments and applying the Fourier transform to each segment, capturing the time-varying frequency content of the signal.

$$V_f^g(t,\eta) = \int_{-\infty}^{+\infty} x(\tau)\omega(\tau - t)e^{-j2\pi f\tau}d\tau \tag{1}$$

where $V_f^g(t,\eta)$ is the STFT of the signal $f(\tau)$, $x(\tau)$ is the signal being analyzed, $\omega(\tau - t)$ is a window function, and $e^{-j2\pi f\tau}$ represents the complex exponential basis functions used in the Fourier transform [34].

For practical applications involving discrete signals, the discrete form of the STFT is described as follows [34]

$$V_f^g(m,k) = \sum_{n=-\infty}^{\infty} x[n]w[n-m]e^{\frac{-j2\pi kn}{N}} \tag{2}$$

where $x[n]$ is the discrete signal, $w[n-m]$ is the discrete window function, k is the frequency bin index, and N is the number of points in the Fourier transform.

One of the main concepts in STFT is the trade-off between time resolution (Δt) and frequency resolution Δf. This is governed by the Heisenberg Uncertainty Principle in signal processing:

$$\Delta t \cdot \Delta f \geq \frac{1}{4\pi} \tag{3}$$

This inequality establishes a strict limitation: improving time resolution results in a degradation of frequency resolution, and vice versa. The choice of window length L directly influences this balance:

Short Window (High Time Resolution): A short analysis window provides precise localization in time, allowing the detection of transient events or rapid changes in the signal. However, the shorter the window, the broader its frequency spectrum, leading to poorer frequency resolution.

Long Window (High Frequency Resolution): A longer analysis window sharpens the frequency resolution, making it suitable for identifying stable or harmonic frequency components. However, this improvement comes at the expense of reduced time resolution, as the window spans over longer periods, blurring rapid time-domain events.

The spectrogram is one of the most common tools used to visualize the results of the STFT. It represents the time-varying frequency content of a signal by plotting the magnitude of the STFT squared

$$S(t,\eta) = \left|V_f^g(t,\eta)\right|^2 \tag{4}$$

where $V_f^g(t,\eta)$ is the STFT of the signal, computed using a window function $g(t)$, t represents time, η denotes frequency, and $\left|V_f^g(t,\eta)\right|^2$ corresponds to the power or energy at a specific time t and frequency η.

2.2. Fourier-Based Synchrosqueezing Transform

FSST is an advanced signal analysis technique that enhances the Time-Frequency (TF) resolution compared to traditional STFT. By more accurately adjusting the frequency components, FSST provides a clearer and more detailed representation of a signal's structure, making it particularly useful for analyzing complex and non-stationary signals where precise TF localization is crucial [35,36].

The instantaneous frequency of the signal at time t and frequency f is calculated as

$$\widetilde{\Omega}[t,f] = \frac{\partial_t V_f^g(t,\eta)}{2i\pi V_f^g(t,\eta)} \tag{5}$$

To apply the FSST effectively, certain specific conditions must first be satisfied for a multicomponent signal (MCS). These conditions ensure that the signal is well suited for precise time-frequency analysis and that the synchrosqueezing process can achieve its intended goal of energy reassignment with high accuracy.

The first condition for applying FSST is that the amplitude $A_k(t)$ must be continuously differentiable $\left(A_k \in C^1(\mathbb{R})\right)$ and bounded $\left(A_k \in L^\infty(\mathbb{R})\right)$. It must also be strictly positive:

$$A_k(t) > 0, \forall t \in \mathbb{R} \tag{6}$$

Additionally, the amplitude must vary slowly over time, satisfying

$$\left|A_k'(t)\right| \leq \epsilon, \forall t \in \mathbb{R} \tag{7}$$

The second condition concerns the phase $\phi_k(t)$ of each signal component. The phase must be twice continuously differentiable $\left(\phi_k \in C^2(\mathbb{R})\right)$ to ensure smooth and gradual variations. Its first derivative, representing the instantaneous frequency, must always be positive and bounded:

$$\phi_k'(t) > 0 \text{ and } \sup_{t\in\mathbb{R}} \phi_k'(t) < \infty \tag{8}$$

Additionally, the second derivative of the phase, $\phi_k''(t)$, which indicates the rate of change in the instantaneous frequency, must also vary slowly:

$$\left|\phi_k''(t)\right| \leq \epsilon, \forall t \in \mathbb{R} \tag{9}$$

The final condition ensures that the frequency separation between adjacent components is sufficiently large to avoid overlapping. Specifically, the difference between the instantaneous frequencies of consecutive components must satisfy the following:

$$\phi'_{k+1}(t) - \phi'_k(t) \geq 2\Delta \tag{10}$$

Using threshold γ and accuracy λ, the FSST of f is defined by [35]

$$T_f^{\gamma,\lambda}(\omega, t) = \frac{1}{g(0)} \int\limits_{|V_f^g(t,\eta)|>\gamma} V_f^g(t,\eta) \frac{1}{\lambda} h\left(\frac{\Omega - \hat{\Omega}[t,f]}{\lambda}\right) df \tag{11}$$

If λ and γ approach zero, $T_f^{\gamma,\lambda}(\omega, t)$ converges to a specific value, which we formally express as

$$T_f(\omega, t) = \frac{1}{g(0)} \int\limits_R X(t,f)\delta\left(\Omega - \hat{\Omega}[t,f]\right) df \tag{12}$$

referred to as FSST in the following, where δ denotes the Dirac distribution.

2.3. Downsampled Discrete STFT

The Downsampled Discrete STFT improves computational efficiency by combining downsampling factors H_t and frequency downsampling factors H_f. This technique is particularly suitable for analyzing large-scale vibration signals while maintaining the essential features of TF analysis [32].

$$S_x^g[m,k] = \sum_{n\in\mathbb{Z}} x[n]g[n - mH_t]e^{\frac{-\mathrm{i}2\pi k(n - mH_t)H_f}{N}} \tag{13}$$

where m and k are time and frequency sequence, H_t and H_f are the two downsampling factors, and N is the sampling point.

For practical implementation, assuming that the discrete window $g[n]$ is consistent for every step and has a support range of $[0, L-1]$, the convolution simplifies into the form of a Discrete Fourier Transform (DFT)

$$S_s^g[m,k] = \sum_{n=0}^{L-1} x[n+mH_t-M]g[n-M]e^{-j2\pi(k-mH_f)/N_f} \tag{14}$$

where $M = (L-1)/2$.

To simultaneously enhance the frequency resolution while maintaining computational efficiency, the number of DFT points, N_f, is chosen so that

$$L = 2M+1 \leq N_f \equiv N \tag{15}$$

This results in the refined formulation:

$$S_s^g[m,k] = e^{j2\pi mH_f/N_f} \sum_{n=0}^{N_f-1} x[n+mH_t-M]g[n-M]e^{-j2\pi kn/N_f} \tag{16}$$

Furthermore, the computation of the DFT in Equation (16) can be accelerated by selecting N_f as a power of 2, enabling the use of the FFT algorithm.

2.4. Reassignment Method

The reassignment method (RM) aims to enhance the clarity of TF representations by repositioning calculated values to improve the concentration of signal components, thereby reducing misleading interference terms [37]. This improves the accuracy of analyzing and classifying non-stationary signals [38]. Reassignment parameters are calculated as follows:

First, we calculate the reassignment parameters:

$$\begin{aligned} \hat{t}(t,\omega) &= t - \frac{\Re(\partial_\eta V_f^g(t,\eta))}{\left|V_f^g(t,\eta)\right|}, \\ \hat{\eta}(t,\omega) &= \omega - \frac{\Re(\partial_t V_f^g(t,\eta))}{\left|V_f^g(t,\eta)\right|} \end{aligned} \tag{17}$$

The STFT $V_f^g(t,\eta)$ is reassigned to a new position $(\hat{t}(t,\omega), \hat{\eta}(t,\omega))$ using these reassignment parameters

$$MS(t',\eta') = \iint S(t,\eta)\delta(t'-\hat{t}(t,\eta)) \cdot \delta(\eta'-\hat{\eta}(t,\eta))dt\frac{d\eta}{2\pi} \tag{18}$$

where $S(t,\eta)$ is the spectrogram of STFT and $\delta(t)$ denotes the Dirac impulse.

The reassignment process addresses the poor time–frequency concentration of the spectrogram by redistributing energy to more accurate locations. In a standard spectrogram, signal energy is often dispersed, making key components hard to identify due to the inseparable kernel of STFT. Reassignment corrects this by relocating energy to its true instantaneous frequency and time, resulting in sharper and more precise time-frequency representations, particularly for analyzing non-stationary signals.

2.5. Downsampled Synchrosqueezing Transform

To clearly outline the steps of DSST, Figure 1 will be designed as a flowchart detailing each phase of the proposed approach.

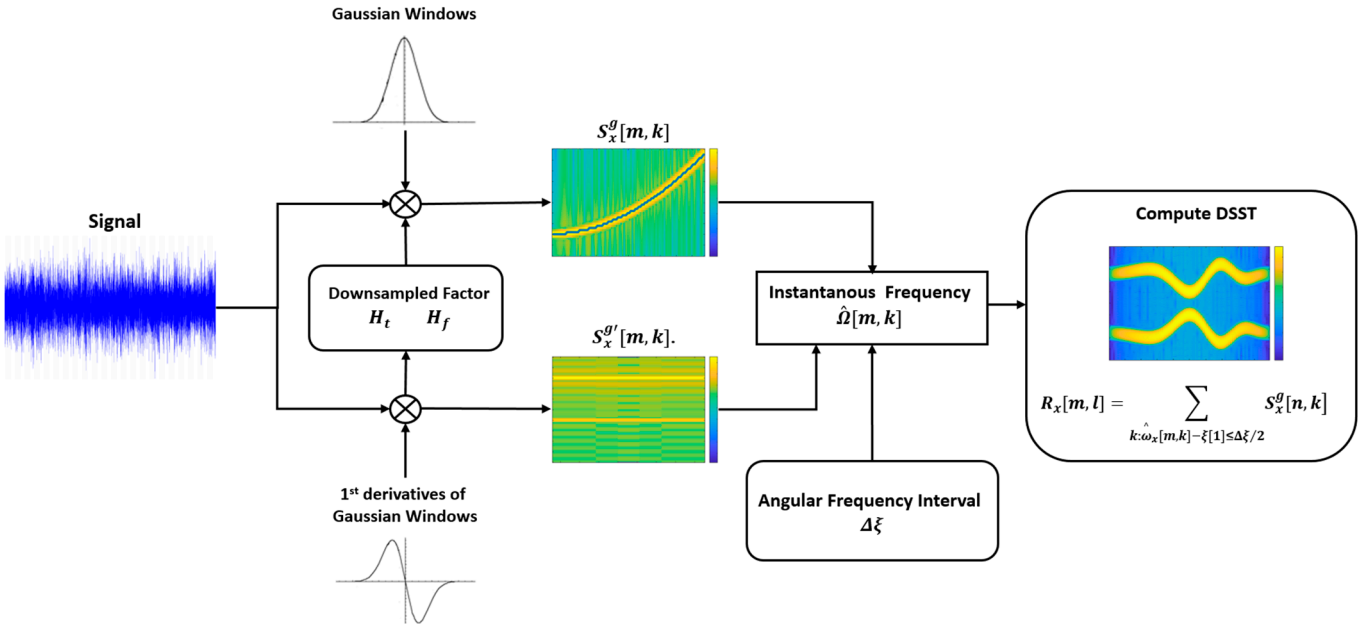


Figure 1. Overview of the proposed DSST-based data-driven diagnostic framework.

The DSST process begins with the application of two different window functions, $g[n]$ and $g\prime[n]$, where $g\prime[n]$ is sampled from $g'(t) = -(\pi\sigma^2)^{\frac{-1}{4}} e^{\frac{-t^2}{2\sigma^2}}.t/\sigma^2$, to the input signal $x[n]$. These windowed signals are then convolved with the input signal and subsequently downsampled by factors H_t and H_f. The downsampled signals are used to compute the STFT, represented as $S_x^g[m,k]$ and $S_x^{g\prime}[m,k]$.

In the reassignment process, the discrete instantaneous frequency (IF) estimator $\hat{\Omega}[m,k]$ for the signal $x[n]$ is calculated using the angular frequency interval $\Delta\xi$, expressed as

$$\Delta\xi = 2\pi\Delta f = \frac{2\pi f_s}{N_f} \tag{19}$$

where $\xi[k] = k\Delta\xi$ is the discrete angular frequency sequence for $k = 0, 1, \ldots, N-1$.

The estimator $\hat{\Omega}[m,k]$ is derived by combining the two STFTs $S_x^g[m,k]$ and $S_x^{g'}[m,k]$ as follows

$$\hat{\Omega}[m,k] = \left|\xi[k] - \Im\left\{\frac{S_x^{g'}[m,k]}{S_x^g[m,k]}\right\}\right|, \text{if } S_x^g[m,k] > \gamma \tag{20}$$

where $\Im[\cdot]$ represents the imaginary part, and γ is the threshold.

This method ensures precise reassignment of time–frequency energy by accurately estimating the instantaneous frequency.

The final reassignment step involves computing the reassigned STFT result by reallocating the TF coefficients based on the estimated instantaneous frequency. This process enhances the readability and accuracy of the TF representation of the signal.

$$R_x[m,l] = \sum_{k:\hat{\omega}_x[m,k]-\xi[1]\leq\Delta\xi/2} S_x^g[n,k] \tag{21}$$

3. Results and Discussion

To validate the proposed method, experimental data from a group at Tsinghua University was utilized [39]. The vibration signal collection process spans 40 s. Initially, the shaft speed is 3000 RPM for 10 s, then it decreases to 2500 RPM over the next 5 s, remains constant

for 10 s, increases back to 3000 RPM in 5 s, and remains stable for the final 10 s (Figure 2). The accelerometer's sampling frequency is set at 12,800 Hz, and the electromagnetic brake load is fixed at 2 Nm.

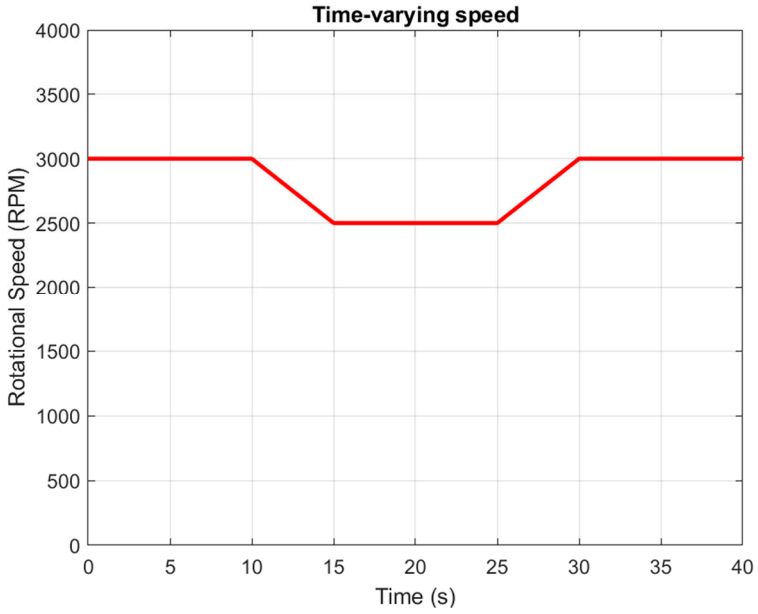


Figure 2. Datasets speed description.

Figure 3 illustrates the spectrograms corresponding to four distinct gear conditions: healthy gear, gear pitting, missing teeth, and broken teeth. These spectrograms, derived using MATLAB's Short-Time Fourier Transform, depict the time-varying frequency content of vibration signals collected over a 40 s window. As seen in all four cases, the gear mesh frequency (GMF) is not constant but changes over time, reflecting the non-stationary nature of the rotating system due to variations in shaft speed. This observation underscores the need for high-resolution time–frequency analysis techniques that are not only capable of accurately tracking time-varying spectral components but also efficient enough to process large-scale vibration data collected over extended monitoring periods.

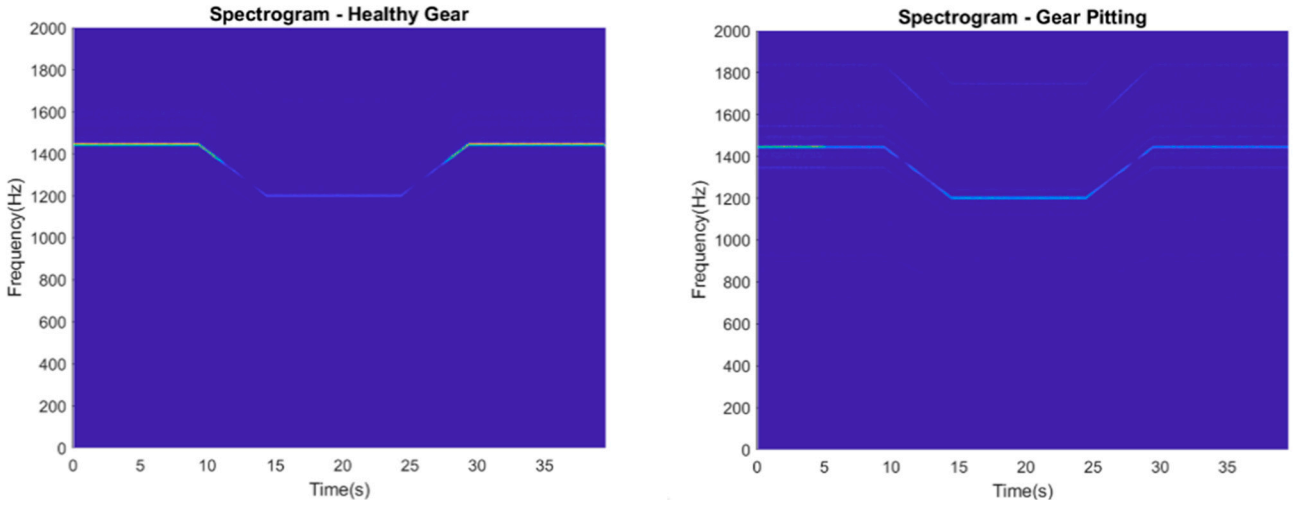


Figure 3. *Cont.*

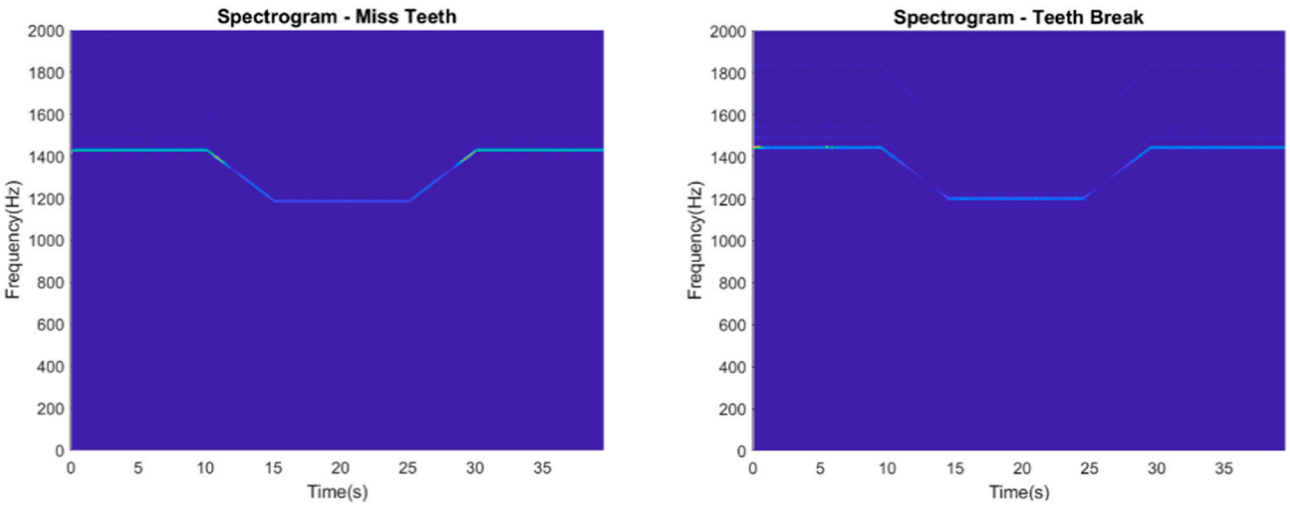


Figure 3. Spectrogram of 4 different gear fault cases.

While the GMF remains visually prominent, the spectrogram fails to resolve finer structures, particularly the sidebands associated with localized gear faults. In the gear pitting and teeth break conditions, these sidebands, critical for differentiating fault types, are only faintly visible or almost completely smeared. In the cases of missing or broken teeth, the differences in spectral behavior are subtle and hard to discern using the spectrogram alone.

This loss of diagnostic detail is a direct result of the STFT's fixed window length, which imposes a trade-off between time and frequency resolution. When applied to long-duration signals with non-stationary content, the spectrogram distributes energy across broader frequency bands, making it difficult to isolate transient or overlapping components. As such, while spectrograms provide a general overview of frequency evolution, their limited resolution restricts their utility for precise fault classification under varying operational conditions.

Figure 4 presents the time–frequency spectra obtained using the FSST for the same vibration datasets. In contrast to the spectrogram results in Figure 3, FSST provides a significantly sharper and more concentrated time–frequency representation. It successfully reveals both the gear mesh frequency (GMF) and its associated sidebands with greater clarity and continuity, especially in periods where rotational speed varies. These improvements directly address the limitations of STFT-based spectrograms, which suffer from energy smearing due to fixed window lengths and limited adaptability to non-stationary components. As such, FSST proves to be a powerful analytical tool for revealing transient and modulated features that are critical for fault diagnosis in rotating machinery.

However, this enhancement in diagnostic fidelity comes with considerable computational overhead. In practical implementation, generating a single FSST-based time–frequency spectrum for a 40 s vibration signal can take up to 60 min, even on a modern workstation. This prolonged processing time stems from FSST's need to compute dense time–frequency grids and perform high-resolution reassignment operations across the entire frequency range. The algorithm must estimate instantaneous frequencies at each time-frequency bin and then reallocate energy accordingly—operations that are mathematically demanding and computationally intensive.

Moreover, FSST's high memory consumption further restricts its usability in embedded or real-time systems. As the length of the input signal increases or higher resolution is required, memory demands grow exponentially, making the method unsuitable for deployment on edge devices or within scalable monitoring infrastructures that must handle hundreds of machines in parallel. Even in high-performance computing environments,

the resource allocation required for FSST limits its applicability in continuous monitoring scenarios, where fast and responsive algorithms are essential.

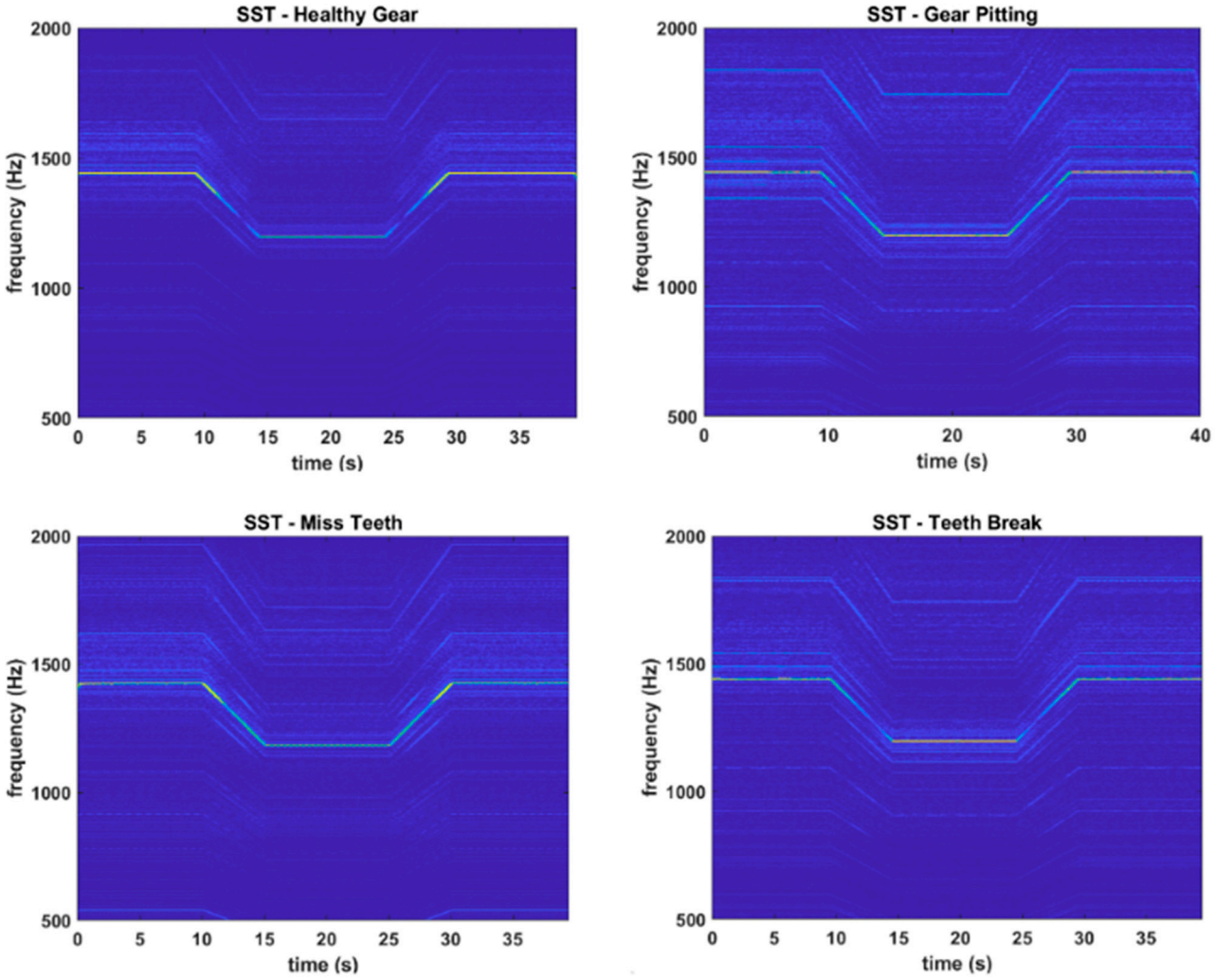


Figure 4. SST of 4 different gear fault cases.

This trade-off between time–frequency resolution and computational efficiency forms the core limitation of FSST in real-world applications. While it undoubtedly surpasses conventional spectrograms in its ability to resolve fine-grained fault features, the method's excessive processing time and hardware dependency create a substantial barrier to its adoption in industry. In modern condition monitoring systems, especially those aligned with Industry 4.0 principles, methods must not only be accurate but also scalable, fast, and lightweight. The inability of FSST to meet these practical requirements highlights a critical need for alternative approaches that retain its diagnostic advantages while mitigating computational costs.

Figure 5a,b illustrates the time–frequency representations obtained using the proposed DSST method for the healthy and gear pitting conditions, respectively. A direct comparison with the results from FSST confirms that DSST maintains a comparable level of resolution, effectively preserving key diagnostic features such as the GMF and its sidebands throughout the duration of the signal. The spectral energy remains well localized, even under non-stationary operating conditions, highlighting the method's robustness in tracking dynamic frequency variations. Most importantly, this level of diagnostic clarity is achieved with a drastically reduced computational burden. In contrast to FSST, which requires up to 60 min of processing time per dataset, DSST performs the full analysis in

a matter of seconds. This efficiency stems from the structured downsampling strategy implemented in both time and frequency domains, which significantly reduces the size of the time–frequency matrix without sacrificing spectral fidelity. The method strategically focuses computational resources on the most informative regions of the signal, making it suitable for deployment in real-time systems and on resource-constrained platforms. The DSST results not only replicate the interpretability of FSST but also demonstrate enhanced practicality. In the gear pitting case (Figure 5b), sidebands around the GMF are clearly distinguishable and sharply defined—an essential criterion for early and accurate fault classification. The method's ability to preserve such features while dramatically reducing computation time underscores its superiority over existing high-resolution transforms. In summary, DSST achieves a critical balance between diagnostic resolution and processing efficiency. It provides a high-fidelity time–frequency representation necessary for fault identification, while enabling scalable, low-latency implementation suitable for modern industrial monitoring environments. These findings establish DSST as a significant advancement over prior approaches, addressing both the computational limitations of FSST and the interpretability shortcomings of traditional STFT-based methods.

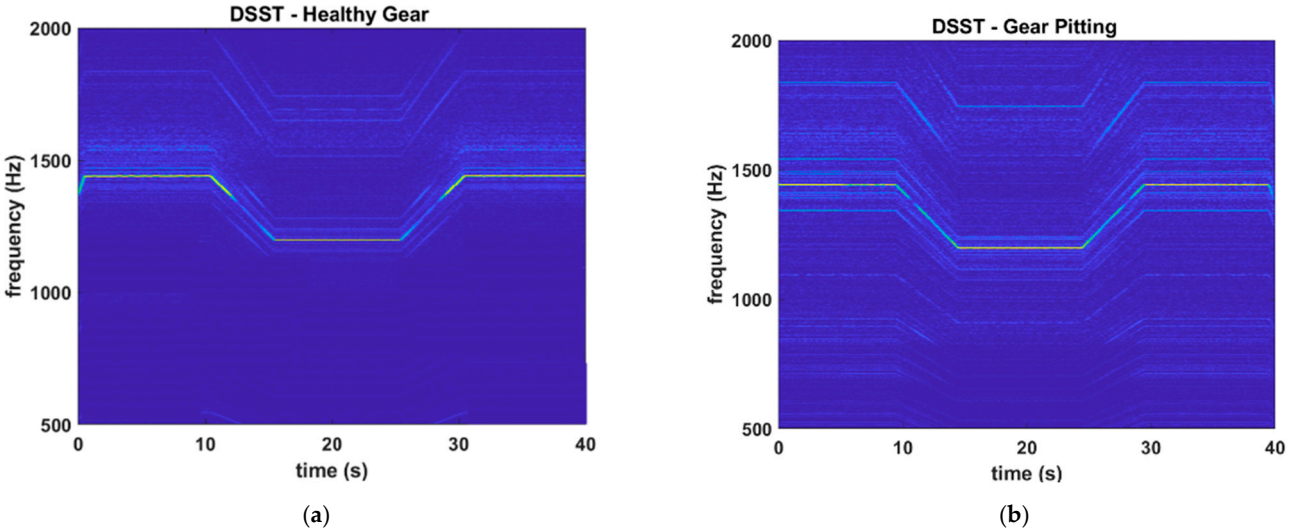


Figure 5. Comparing in case of healthy gear (**a**) and pitting gear (**b**).

To further substantiate the effectiveness of the proposed method, Figures 6 and 7 provide magnified views of the time–frequency spectra previously shown in Figure 5, focusing on representative fault cases. These zoomed-in visualizations allow for closer inspection of the spectral features associated with healthy and pitting gear conditions, revealing the diagnostic detail captured by DSST with improved clarity.

In Figure 6, corresponding to the healthy gear case, the GMF is distinctly visible as a clean and continuous ridge without the presence of surrounding sidebands—an expected spectral signature in the absence of faults. This result confirms that DSST accurately preserves fundamental gear dynamics while avoiding false indications of damage. By contrast, Figure 7 illustrates the gear pitting scenario and clearly exhibits multiple sidebands distributed both above and below the GMF. These spectral components are characteristic of amplitude and frequency modulations induced by localized tooth damage. The visibility of both upper and lower sidebands in the time–frequency plane underscores the method's sensitivity to fault-induced modulations. Importantly, despite being visualized at a high time downsampling factor, the DSST results maintain sharp spectral concentration, demonstrating that critical diagnostic features are retained even under aggressive computational simplification. Together, these figures reinforce that DSST not only captures the essential

fault-related features necessary for accurate diagnosis but does so in a computationally efficient manner. The method strikes a highly effective balance between spectral resolution and processing cost, enabling the reliable identification of gear faults under non-stationary conditions with minimal sacrifice in interpretability.

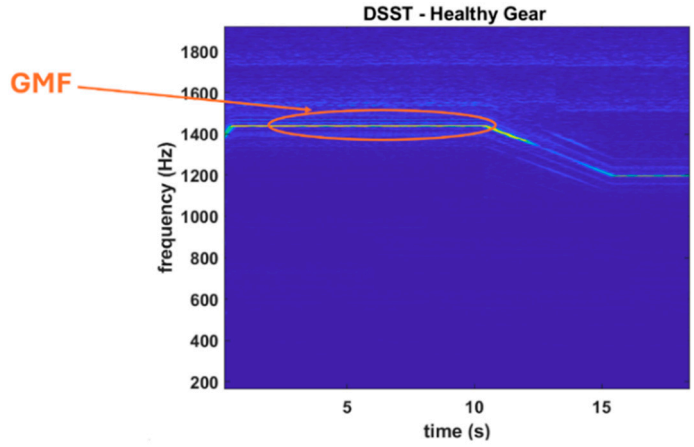


Figure 6. The proposed method detects healthy gear with GMF.

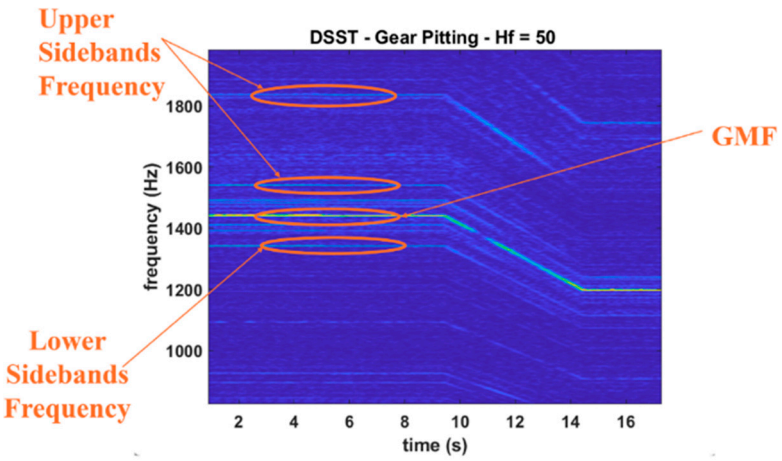


Figure 7. The proposed method detects pitting gear with GMF and sidebands.

Figure 8 displays the results of the DSST transform applied to the gear pitting case with different time downsampling factors (H_t = 1, 20, 50), while keeping the frequency downsampling factor constant (H_f = 1). From a visual perspective, increasing H_t has minimal impact on the concentration or readability of the time–frequency representation (TFR). The GMF and its sidebands remain clearly identifiable across all cases, confirming that the diagnostic features are preserved.

However, computational efficiency improves significantly as H_t increases. For example, with H_t = 50, the processing time is drastically reduced compared to H_t = 1, while maintaining comparable resolution. This demonstrates the effectiveness of DSST in balancing computational efficiency with diagnostic accuracy. Furthermore, when compared to SST, the DSST method provides similar TFR clarity, emphasizing its capability to process large-scale vibration data with reduced computational load.

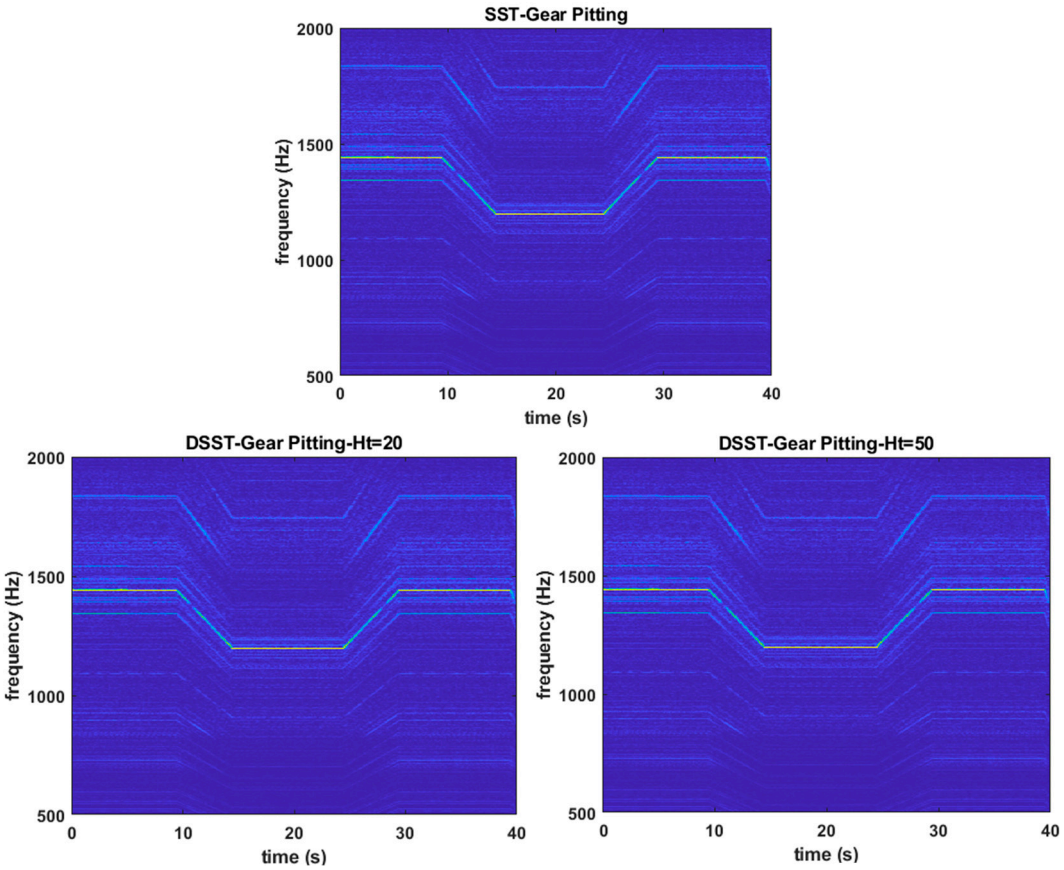


Figure 8. Comparison of TFR between SST and DSST with different time downsampling factors H_t.

However, the most significant difference is shown in Table 1, where the elapsed time is considerably reduced compared to SST, 3.45 s, when H_t = 20 and 1.15 s when H_t = 50. The time cost in the second row is nearly half that of the first row, as the number of DFT points is halved. Similarly, the time cost in the second and third columns is about 1/20 and 1/50 of that in the first column, respectively. This demonstrates the efficiency of the proposed method in minimizing computational complexity while retaining the characteristic damage values.

Table 1. Computation time of DSST with varying downsampling factors H_t.

H_f	H_t		
1	1	20	50
	60.45	3.45	1.15

Table 1 highlights the significant improvement in computational efficiency achieved by the DSST method with different time downsampling factors (H_t). When H_t = 1, the elapsed time is 60.45 s, equivalent to the computational time of SST. However, by increasing H_t to 20, the elapsed time reduces dramatically to 3.45 s, approximately 1/20 of the initial time. Further increasing H_t to 50 reduces the processing time to just 1.15 s, roughly 1/50 of the original duration.

This reduction in time is directly correlated with the number of DFT points processed, as increasing H_t effectively decreases the size of the time-domain data. Despite this drastic reduction in computational load, the diagnostic capability of DSST remains intact, as shown in the previous figures. The method successfully retains critical features such as the GMF and sidebands, which are essential for fault diagnosis.

Figure 9 continues to illustrate the results of the DSST method with the gear pitting data when changing the H_f factor. The elapsed time of the algorithm continues to demonstrate the efficiency of the proposed method, with the SST transform taking up to 59.98 s to process, while the DSST transform with $H_f = 20$ takes 3.75 s and with $H_f = 50$ takes 1.27 s, as shown in Table 2. However, unlike when changing the H_t coefficient, the resolution of TF representation is not significantly affected. When changing the H_f coefficient, the resolution decreases significantly. To quantitatively assess the impact of the downsampling factor on the concentration of TFR, particularly when using a relatively large factor, Rényi entropy is used. This entropy quantifies the concentration of the TFRs produced by fully sampled SST, downsampled SST, and STFT.

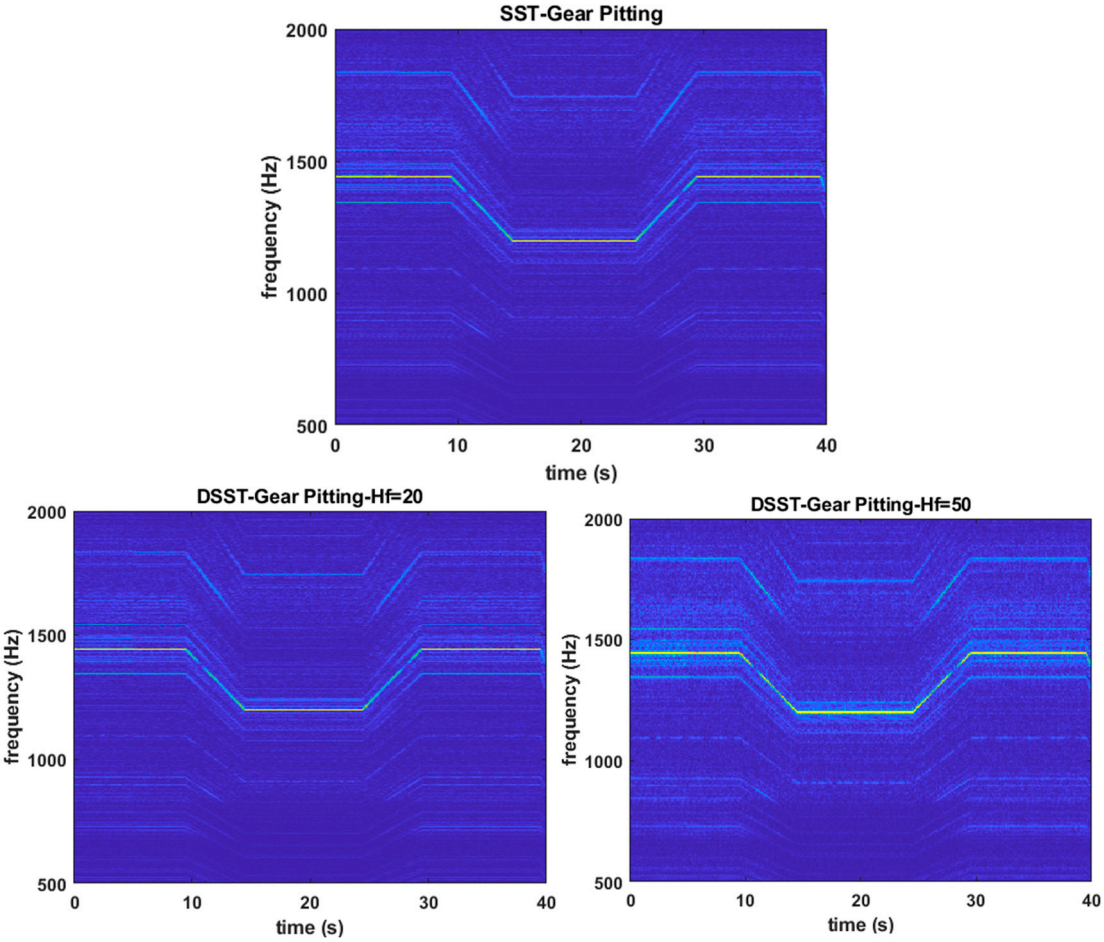


Figure 9. Comparison of TFR between SST and DSST with different frequency downsampling factor H_f.

Table 2. The computation time of DSST with varying downsampling factors H_f.

H_f	H_t		
1	1	20	50
	59.98	3.75	1.27

The Rényi entropy of order α for a TFR $P(u, \xi)$ is described as [40,41]

$$R_P^{\alpha} = \frac{1}{1-\alpha} \log_2 \iint \left(P(u,\xi) / \iint P(u,\xi) \mathrm{d}u\mathrm{d}\xi \right)^a \mathrm{d}u\mathrm{d}\xi \tag{22}$$

For SST, the downsampling factors in the time and frequency domains influence concentration in distinct ways. The entropy of SST remains stable with changes in H_t but rises significantly with increases in H_f. This is because H_f has a more substantial effect on SST concentration due to the reassignment of TF energy along the frequency axis.

4. Conclusions

This study introduces the data-driven synchrosqueezing-based signal transformation (DSST) as a robust and scalable solution for gearbox fault diagnosis under non-stationary operating conditions. By integrating synchrosqueezing theory with structured downsampling in both time and frequency domains, DSST achieves a substantial reduction in computational complexity while preserving the high-resolution characteristics essential for detecting diagnostic features such as gear meshing frequency harmonics and sidebands. Distinct from prior works, which emphasized algorithmic efficiency without embedding the method in a diagnostic context, this study advances the state-of-the-art by formulating DSST as a practical and interpretable module compatible with real-time, resource-constrained, and data-driven condition monitoring systems.

The proposed framework not only retains the capacity for accurate signal reconstruction but also produces compact, feature-rich time–frequency representations that are directly applicable to downstream machine learning tasks. Through experimental validation on non-stationary gearbox vibration signals, DSST demonstrates diagnostic performance comparable to conventional SST techniques while enabling real-time deployment, particularly in edge computing scenarios. These results underscore the method's potential for scalable implementation in Industry 4.0 environments, where rapid and interpretable fault detection is critical. Despite its advantages, the performance of DSST remains sensitive to the choice of downsampling parameters, which may affect its ability to capture weak or transient fault signatures. Additionally, the current implementation focuses primarily on broad fault identification; further research will explore adaptive parameter optimization and integration with end-to-end deep learning architectures for a more refined fault classification. Overall, DSST represents a significant advancement toward intelligent, efficient, and interpretable condition monitoring in complex industrial systems.

Author Contributions: N.-P.H.: Writing—original draft, Writing—review and editing, Formal Analysis, Investigation, Methodology, Software. T.-D.N.: Conceptualization, Formal Analysis, Investigation, Methodology, Software, Writing—original draft, Writing—review and editing, Supervision, Validation. T.-V.-H.N.: Conceptualization, Investigation, Software, Visualization, Writing—original draft, Data curation. D.-H.P.: Writing—review and editing, Visualization, Data curation. P.-D.N.: Data curation, Funding acquisition, Methodology, Project administration, Resources, Supervision, Validation, Writing—review and editing. T.-H.N.: Writing—review and editing, Visualization, Data curation. All authors have read and agreed to the published version of the manuscript.

Funding: This research is funded by Hanoi University of Science and Technology (HUST) under project number T2024-PC-018.

Data Availability Statement: Data are contained within the article.

Conflicts of Interest: The authors declare no conflicts of interest.

References

1. Goswami, P.; Nandan Rai, R. A systematic review on failure modes and proposed methodology to artificially seed faults for promoting PHM studies in laboratory environment for an industrial gearbox. *Eng. Fail. Anal.* **2023**, *146*, 107076. [CrossRef]
2. Mohd Ghazali, M.H.; Rahiman, W. Vibration Analysis for Machine Monitoring and Diagnosis: A Systematic Review. *Shock Vib.* **2021**, 1–25. [CrossRef]

3. Matania, O.; Bachar, L.; Khemani, V.; Das, D.; Azarian, M.H.; Bortman, J. One-fault-shot learning for fault severity estimation of gears that addresses differences between simulation and experimental signals and transfer function effects. *Adv. Eng. Inform.* **2023**, *5*, 101945. [CrossRef]
4. Du, N.T.; Dien, N.P.; Nga, N.T.T. Gear fault detection in gearboxes operated in non-stationary conditions based on variable sideband analysis without a tachometer. *Front. Mech. Eng.* **2022**, *8*, 1021222. [CrossRef]
5. Feng, K.; Ji, J.C.; Ni, Q.; Beer, M. A Review of Vibration-based Gear Wear Monitoring and Prediction Techniques. *Mech. Syst. Signal Process.* **2023**, *182*, 109605. [CrossRef]
6. Salameh, J.P.; Cauet, S.; Etien, E.; Sakout, A.; Rambault, L. Gearbox condition monitoring in wind turbines: A review. *Mech. Syst. Signal Process.* **2018**, *111*, 251–264. [CrossRef]
7. Aherwar, A.; Khalid, M.S. Vibration analysis techniques for gearbox diagnostics: A review. *Int. J. Adv. Eng. Technol.* **2012**, *III*, 4–12.
8. Nguyen, T.-D.; Nguyen, P.-D. Improvements in the Wavelet Transform and Its Variations: Concepts and Applications in Diagnosing Gearbox in Non-Stationary Conditions. *Appl. Sci.* **2024**, *14*, 4642. [CrossRef]
9. Dai, P.; Wang, J.; Lu, J.; Yan, S.; Qian, Z.; Wang, F. Vibration characteristics analysis of spur gear pair with crack fault under variable working conditions. *Zhendong Yu Chongji/J. Vib. Shock* **2022**, *41*, 225–234. [CrossRef]
10. Wilke, D.N.; Schmidt, S.; Heyns, P.S. A Review of Singular Spectral Analysis to Extract Components from Gearbox Data. In *Modelling and Simulation of Complex Systems for Sustainable Energy Efficiency (MOSCOSSEE 2021)*; Applied Condition Monitoring; Springer: Cham, Switzerland, 2022. [CrossRef]
11. Gu, H.; Liu, W.Y.; Gao, Q.W.; Zhang, Y. A review on wind turbines gearbox fault diagnosis methods. *J. Vibroeng.* **2021**, *23*, 26–43. [CrossRef]
12. Dien, N.P.; Du, N.T. Fault Detection for Rotating Machines in Non-stationary Operations Using Order Tracking and Cepstrum. In *Advances in Engineering Research and Application*; Nguyen, D.C., Vu, N.P., Long, B.T., Puta, H., Sattler, K.-U., Eds.; Springer International Publishing: Cham, Switzerland, 2020; pp. 349–356.
13. Cempel, C.; Tabaszewski, M. Multidimensional condition monitoring of machines in non-stationary operation. *Mech. Syst. Signal Process* **2007**, *21*, 1233–1241. [CrossRef]
14. Randall, R.B. *Vibration-Based Condition Monitoring: Industrial, Aerospace and Automotive Applications*; Wiley: Hoboken, NJ, USA, 2010. [CrossRef]
15. Akram, M.A.; Khushnood, S.; Tariq, S.L.; Ali, H.M.; Nizam, L.A. Vibration Based Gear Fault Diagnosis under Empirical Mode Decomposition and Power Spectrum Density Analysis. *Adv. Sci. Technol. Res. J.* **2019**, *13*, 192–200. [CrossRef] [PubMed]
16. Pan, J.; Chen, J.; Zi, Y.; Li, Y.; He, Z. Mono-component feature extraction for mechanical fault diagnosis using modified empirical wavelet transform via data-driven adaptive Fourier spectrum segment. *Mech. Syst. Signal Process.* **2016**, *72–73*, 160–183. [CrossRef]
17. Zhao, D.Z.; Li, J.Y.; Cheng, W.D. Fault diagnosis of rolling bearing under gear noise interference and variable rotating speed. *Huanan Ligong Daxue Xuebao/J. South China Univ. Technol. (Nat. Sci.)* **2016**, *44*, 67–73. [CrossRef]
18. Zhang, X.; Xu, G.; Kuang, J.; Suo, L.; Zhang, S.; Khalique, U. A three-phase current tacholess envelope order analysis method for feature extraction of planetary gearbox under variable speed conditions. *Sensors* **2021**, *21*, 5714. [CrossRef]
19. Randall, R.B. Vibration-based diagnostics of gearboxes under variable speed and load conditions. *Meccanica* **2016**, *51*, 3227–3239. [CrossRef]
20. Du, N.T.; Dien, N.P. Advanced Signal Decomposition Methods for Vibration Diagnosis of Rotating Machines: A Case Study at Variable Speed. In *Modern Mechanics and Applications*; Lecture Notes in Mechanical Engineering; Springer: Singapore, 2022. [CrossRef]
21. Pachori, R.B. *Time-Frequency Analysis Techniques and Their Applications*; Taylor & Francis: London, UK, 2023. [CrossRef]
22. Sun, R.; Yang, Z.; Chen, X.; Tian, S.; Xie, Y. Gear fault diagnosis based on the structured sparsity time-frequency analysis. *Mech. Syst. Signal Process.* **2018**, *102*, 346–363. [CrossRef]
23. Mateo, C.; Talavera, J.A. Short-time Fourier transform with the window size fixed in the frequency domain. *Digit. Signal Process. A Rev. J.* **2018**, *77*, 13–21. [CrossRef]
24. Du, J.; Li, X.; Gao, Y.; Gao, L. Integrated Gradient-Based Continuous Wavelet Transform for Bearing Fault Diagnosis. *Sensors* **2022**, *22*, 5760. [CrossRef]
25. Yang, X.W.; Chen, J.; Zheng, S.P.; Cai, Z.W. Application research of continuous wavelet transform in crack fault diagnosis of transmission gear. In Proceedings of the International Computer Conference on Wavelet Active Media Technology and Information, Chongqing, China, 29–31 August 2006; pp. 1161–1168.
26. Gaurav Thakur, H.-T.W. Synchrosqueezing-based Recovery of Instantaneous Frequency from nonuniform Samples. *Int. J. Appl. Math.* **2011**, *43*, 2078–2095.
27. Oberlin, T.; Meignen, S.; Perrier, V. The fourier-based synchrosqueezing transform. In Proceedings of the ICASSP, IEEE International Conference on Acoustics, Speech and Signal Processing—Proceedings, Florence, Italy, 4–9 May 2014. [CrossRef]
28. Daubechies, I.; Lu, J.; Wu, H.T. Synchrosqueezed wavelet transforms: An empirical mode decomposition-like tool. *Appl. Comput. Harmon. Anal.* **2011**, *30*, 243–261. [CrossRef]

29. Li, C.; Liang, M. Timefrequency signal analysis for gearbox fault diagnosis using a generalized synchrosqueezing transform. *Mech. Syst. Signal Process.* **2012**, *26*, 205–217. [CrossRef]
30. Pham, D.H.; Meignen, S. High-Order Synchrosqueezing Transform for Multicomponent Signals Analysis-With an Application to Gravitational-Wave Signal. *IEEE Trans. Signal Process.* **2017**, *65*, 3168–3178. [CrossRef]
31. Liu, W.; Chen, W.; Zhang, Z. A Novel Fault Diagnosis Approach for Rolling Bearing Based on High-Order Synchrosqueezing Transform and Detrended Fluctuation Analysis. *IEEE Access* **2020**, *8*, 12533–12541. [CrossRef]
32. He, D.; Cao, H. Downsampling-based synchrosqueezing transform and its applications on large-scale vibration data. *J. Sound Vib.* **2021**, *496*, 115938. [CrossRef]
33. Mateo, C.; Talavera, J.A. Short-Time Fourier Transform with the Window Size Fixed in the Frequency Domain (STFT-FD): Implementation. *SoftwareX* **2018**, *8*, 5–8. [CrossRef]
34. Pachori, R.B. Short-Time Fourier Transform. In *Time-Frequency Analysis Techniques and their Applications*; Taylor & Francis: London, UK, 2023. [CrossRef]
35. Behera, R.; Meignen, S.; Oberlin, T. Theoretical analysis of the second-order synchrosqueezing transform. *Appl. Comput. Harmon. Anal.* **2018**, *45*, 379–404. [CrossRef]
36. Li, Z.; Gao, J.; Li, H.; Zhang, Z.; Liu, N.; Zhu, X. Synchroextracting transform: The theory analysis and comparisons with the synchrosqueezing transform. *Signal Process.* **2020**, *166*, 107243. [CrossRef]
37. Yu, G.; Yu, M.; Xu, C. Synchroextracting Transform. *IEEE Trans. Ind. Electron.* **2017**, *64*, 8042–8054. [CrossRef]
38. Wei, D.; Huang, Z.; Mao, H.; Li, X.; Huang, H.; Wang, B.; Yi, X. Iterative reassignment: An energy-concentrated time-frequency analysis method. *Mech. Syst. Signal Process.* **2023**, *182*, 109579. [CrossRef]
39. Chen, S.; Liu, Z.; He, X.; Zou, D.; Zhou, D. Multi-mode fault diagnosis datasets of gearbox under variable working conditions. *Data Brief* **2024**, *54*, 110453. [CrossRef] [PubMed]
40. Baraniuk, R.G.; Flandrin, P.; Janssen, A.; Michel, O. Measuring time-frequency information content using the Reényi entropies. *IEEE Trans. Inf. Theory* **2001**, *47*, 1391–1409. [CrossRef]
41. Chen, M.; Yu, D.; Gao, Y. Fault diagnosis of rolling bearings based on graph spectrum amplitude entropy of visibility graph. *Zhendong Yu Chongji/J. Vib. Shock* **2021**, *40*, 23–29. [CrossRef]

Disclaimer/Publisher's Note: The statements, opinions and data contained in all publications are solely those of the individual author(s) and contributor(s) and not of MDPI and/or the editor(s). MDPI and/or the editor(s) disclaim responsibility for any injury to people or property resulting from any ideas, methods, instructions or products referred to in the content.